38th AIAA/ASME/SAE/ASEE Joint Propulsion Conference & Exhibit
7-10 July 2002, Indianapolis, Indiana

AIAA 2002-4050

Electron Collection to Arbitrarily Shaped Electrodynamic Tethers in Flowing Plasmas: a Kinetic Model
Validation for Circular Cross-sections

Eric Choinière* and Brian E. Gilchrist†
University of Michigan, Ann Arbor, Michigan 48109

Tether electron current collection is one of the key mechanisms allowing for power and/or thrust generation applications of space electrodynamic tethers and depends on such parameters as tether geometry and the velocity of plasma flow. This paper presents the initial validation of a novel computational approach, based on kinetic theory, that will allow for the assessment of the efficiency of electron collection to bare tethers of arbitrary cross sections from a flowing space plasma. The drift velocity associated with the translational speed of the tether is incompatible with 1-D, cylindrically symmetric models[1,2] and its effects on current collection are not well understood. A kinetic model is developed for the two-dimensional plasma surrounding the tether, which consists in self-consistently solving the Vlasov and Poisson equations through a semi-analytical, semi-numerical process. A drifting Maxwellian velocity distribution is assumed for the plasma species (electrons and ions) at the outer boundary of the solution space; no assumption is made regarding the velocity distributions in the computational region surrounding the tether, allowing for fully poly-energetic species. Simulation results are validated with Langmuir cylindrical probe theory for the non-flowing case. For flowing cases, some initial results show a qualitative agreement with results from vacuum chamber experiments[g] but further work is needed to improve the consistency of the results. Work is underway to allow the use of the model for arbitrary tether geometries.

Nomenclature

Δv	Range of velocities accounted for on the outer boundary (m/s)
E_x	x component of the electric field (V/m)
E_y	y component of the electric field (V/m)
f_e	Electron velocity distribution
f_i	Ion velocity distribution
$\vec{g}(\cdot)$	Fixed-point nonlinear operator comprising both a Poisson and Vlasov solvers (input in C/m^2, output in C/m^2)
$\vec{h}(\cdot)$	Fixed-point nonlinear operator based on the regularized Newton method
I_{oml}	OML theory-predicted collection current (A)
I_e	Electron current to the probe (A)
$\mathbf{J_g}$	Jacobian matrix of operator $\vec{g}(\cdot)$.
K_{max}	Range of kinetic energies accounted for on the outer boundary (eV)
m_e	Electron mass (kg)
m_i	Ion mass (kg)
n_0	Background plasma density (m^{-3})
OML	Orbital Motion Limit
q_e, e	Electron charge $= +1.6021 \times 10^{-19} C$
q_i	Ion charge (C)
r_0	Probe radius (m)
r	Radial distance measured from the center of the tether conductor (m)
r_{bc}	Radius of outer equipotential shell (m)
$\rho(x,y)$	Net plasma charge density distribution (C/m^2)
$\rho_s(x,y)$	Surface charge density distribution (C/m)
$\vec{\rho}$	Vector containing samples of the charge density distribution at mesh nodes (C/m^2)
T_e	Electron temperature (eV)
T_i	Ion temperature (eV)
v_x	x component of velocity (m/s)
v_y	y component of velocity (m/s)
v_d	2-directed plasma drift velocity (m/s)
V_p	Probe voltage (V)
$v_{min,max}$	Minimum/maximum velocity accounted for at any given position (m/s)
$V(x,y)$	Electric potential distribution (V)
V_{plasma}	Plasma contribution to the electric potential distribution (V)
V_{psc}	Probe surface charge contribution to the electric potential distribution (V)
$\vec{V}$	Vector containing samples of the potential distribution at the specified nodes (V)

*Graduate Student, Radiation Laboratory, EECS Department
†Associate Professor, Electrical Engineering and Space Sciences, AIAA Senior Member

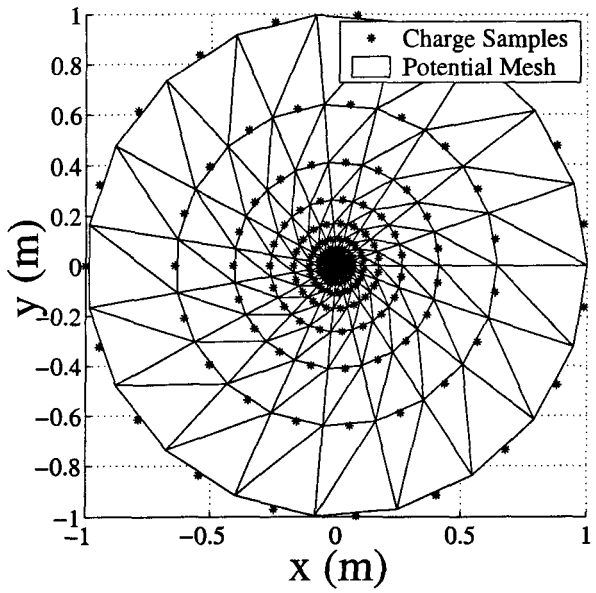

Fig. 2 Triangulation Schemes for the Potential and Charge Distributions.

scribe both solvers and present the iterative scheme that was used.

Vlasov solver

As the following section will show, the Vlasov solver described here allows each species to express the full poly-energetic nature of its velocity distribution, which is what makes the realism and accuracy of the code. For a collisionless species in a quiescent, magnetized plasma, Vlasov's equation in **2-D** can be written **as:**

$$\frac{df}{dt} = v_x \frac{\partial f_{e,i}}{\partial x} + v_y \frac{\partial f_{e,i}}{\partial y} + \frac{q_{e,i} E_x(x,y)}{m_{e,i}} \frac{\partial f_{e,i}}{\partial v_x} + \frac{q_{e,i} E_y(x,y)}{m_{e,i}} \frac{\partial f_{e,i}}{\partial v_y} = 0 \quad (2)$$

Given a known electric field distribution $\vec{E}(x,y)$ and the outer "drifting Maxwellian" boundary condition for the velocity distributions, equation (2) can be used to solve for the velocity distributions $f_{e,i}(x, \mathrm{y}, v_x, v_y)$ of both the electrons and ions. The species densities are then obtained by integrating over all velocity space:

$$n_{e,i} = J \int f_{e,i}(x,y,v_x,v_y) dv_x dv_y \quad (3)$$

and the total charge density results from $\rho(x,y) = q_i n_i - e n_e$.

Equation **(2)** specifies that the distribution function $f_{e,i}(x, \mathrm{y}, v_x, v_y)$ is constant along particle orbits in a given electric field distribution. Using the specified boundary condition for the velocity distribution at the outer shell, the value for $f_{e,i}(x, \mathrm{y}, v_x, v_y)$ for any point and velocity located on a trajectory originating from the outer shell can be inferred. This can be done by

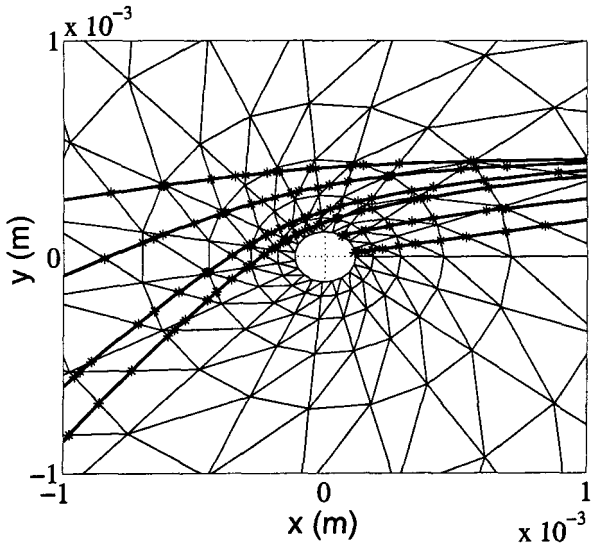

Fig. 3 Example of the Semi-analytical Particle Tracking Process Through the Potential Mesh.

tracking the particle's trajectory back in time until it hits the outer boundary. Any trajectory not originating from the outer shell is deemed unpopulated.' Such is the case for those trajectories originating from the tether itself, which does not emit charged particles, **as** well as trapped trajectories which have no sources of particles in the collisionless case.

Figure **3** illustrates the particle tracking process. The trajectories are tracked analytically from one edge of the mesh to another, assuming a constant electric field within any given triangle of the mesh. Every sub-trajectory is thus resolved by computing the intersection of **a** quadratic parametric curve with a segment on the mesh. This technique is much more efficient than using a fixed time step particle pusher, since the amount of computations necessary for one trajectory depends on the number of edges being crossed rather than the number of time steps necessary to reach a boundary. Also, given the assumption of a piecewise-bilinear potential distribution, it provides exact *(nearly* exact if we account for roundoff errors) conservation of energy along orbits, which contributes to the accuracy of the overall approach.

To obtain a value for the particle density at a given point, one needs to integrate the values obtained for $f_{e,i}(x,y,v_x,v_y)$ using the integral shown in equation **(3).** To limit the computational task, the domain of integration is restricted to a limited region outside of which the velocity distribution function is known to be very low. Knowing that the velocity distribution function anywhere on the outer boundary is given by equation (1), one can invoque conservation of energy to restrict the integration domain to a certain range of kinetic energies. At the outer boundary, a range of integration $K_{max} = \kappa T_{e,i}$ (units of eV's) is specified in terms of the species temperature (typically, $\kappa = 10$).

Introduction

BARE electrodynamic space tethers are under consideration for applications such as power generation and propellantless propulsion for orbiting spacecraft. In these applications, one of the primary concerns is the ability of the system to collect electrons from the surrounding ionospheric plasma in order to maximize the amount of electrical power or thrust provided. This value increases with the magnitude of the current flowing on the tether, which in turn is, in part, limited by the tether's ability to collect electrons from the surrounding plasma.

Analytical models are available'?' for the electron current collection problem in the limiting case of the Orbital Motion Limit regime and a stationary plasma with respect to the probe. A numerical model was also developed' for the general case which was based on a self-consistent, 1-D solution of Vlasov and Poisson's equations for a cylindrically symmetric structure and boundary conditions. This model did not restrict its application to the OML regime, however it allowed neither the inclusion of a plasma drift or arbitrary probe geometries.

This paper presents a novel approach, based on a poly-energetic kinetic model, for the accurate analysis of the electron/ion current collection problem to a bare tether in a collisionless, drifting plasma. This technique is a **2-D** extension of the self-consistent 1-D numerical model developed earlier,' and allows inclusion of a drift velocity to the background plasma as well as opening the possibility for accurate modeling of tethers of arbitrary cross-sections.

We will first provide a physical and mathematical description of the problem under consideration. The proposed iterative resolution scheme will then be introduced, together with the associated computational issues. Finally, we will show the computation results that were obtained and show theoretical validation and qualitative experimental validation of our results.

Description of the 2-D Conducting Tether Problem

Figure 1 presents the basic geometry being considered here. The tether is assumed to be a cylinder of infinite length, surrounded by a plasma comprised of electrons and ions. In the simulation, an outer equipotential shell is placed at a radius r_{bc} from the center of the tether, in order to simulate the background plasma potential and limit the computational region. A potential V_0 with respect to the plasma potential is specified at the probe surface. Although no assumptions are made concerning the velocity distributions of the plasma species within the computational region, it is assumed that both the ion and electron populations have a drifting Maxwellian velocity distribution at the outer shell, that is, in the background plasma:

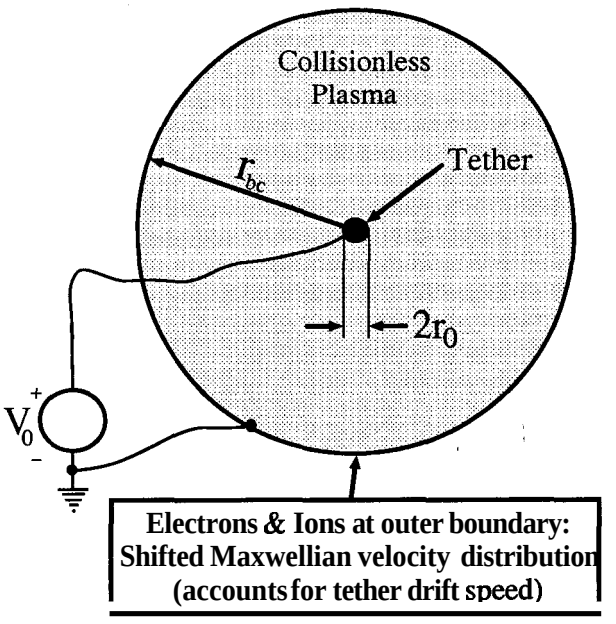

Fig. 1 Basic Geometry of the Artificial Tether Problem.

$$f_{e,i}(v_x, v_y) = \frac{n_0 m_{e,i}}{2\pi e T_{e,i}} \exp\left\{-\frac{m_{e,i}}{2eT_{e,i}}\left((v_x - v_d)^2 + v_y^2\right)\right\} \quad (1)$$

In order to simplify the initial development of the modeling technique, we assume a collisionless, unmagnetized quiescent plasma. Additionally, it is assumed that the electric field vanishes for $r > r_{bc}$ and that the potential distribution is piecewise bilinear. In other words, it varies bilinearly within any of the triangles of the mesh.

As the last assumption specifies, the potential and charge density distributions are sampled on two separate fixed grids of points, which together form a set of adjacent triangles. Figure 2 illustrates the discretization schemes used for both the potential and charge density distributions. The meshes are spaced logarithmically along the radial direction, which is justified by the expected large variations near the tether **as** opposed to the smoother variations further out. The consequence of the bilinearity assumption for the potential is that both components of the electric field, E, and E_y, will be piecewise constant (constant on any single triangle).

Iterative consistent 2-D plasma solver

In order to obtain a consistent solution for the electric fields and the density distributions for both the ion and electron species, we need to solve, self-consistently, Vlasov's equation for each species and Poisson's equation for the electric potential and charges, while satisfying the above-mentioned boundary conditions. An iterative scheme was developed using both a Poisson solver and Vlasov solver. In the following we will de-

probe that will result in a total potential V_0 at all nodes located on the surface of the probe. The "probe surface charge" contribution to the complete plasma distribution is then:

$$V_{psc}(r,\theta) = \frac{-r_0}{4\pi\epsilon_0}\int d\theta' \rho_s(r_0,\theta') \times \left[\ln\left(\frac{r^2 + r_0^2 - 2r_0 r\cos(\theta-\theta')}{r_{bc}^2 + r_0^2 - 2r_0 r_{bc}\cos\theta'}\right) - \ln\left(\frac{r^2 + (r_{bc}^2/r_0)^2 - 2(r_{bc}^2/r_0)r\cos(\theta-\theta')}{r_{bc}^2 + (r_{bc}^2/r_0)^2 - 2(r_{bc}^3/r_0)\cos\theta'}\right)\right] \quad (11)$$

where $\rho_{s(r_0,\theta)}$ is obtained using a point-matching technique' that enforces $V_{psc}(r_0,\theta) + V_{plasma}(r_0,\theta) = V_0$ at all nodes on the probe surface.

The total potential distribution is obtained from the sum of equations (10) and (11). Since the integrals are performed over piecewise bilinear functions, the complete Poisson solver (including the point-matching operation) can be written in the form of a linear matrix operator, which makes it computationally trivial compared to the Vlasov solver:

$$\vec{V} = [\rho 2V]\vec{\rho} + \vec{V}_{cst} \quad (12)$$

Iterative Resolution Technique

Using the Poisson and Vlasov solvers, we seek a solution for the potential and charge distributions that simultaneously satisfies the Poisson and Vlasov equations. Figure 5 depicts the general fixed-point operator comprised of both the Poisson and Vlasov solvers. The fixed-point operator takes a charge distribution $\vec{\rho}_{in}$ at its input and generates a new estimate $\vec{\rho}_{out}$:

$$\vec{\rho}_{out} = \vec{\mathbf{g}}_{(Fin)} \quad (13)$$

There are known difficulties arising in solving such a problem.' Simple iteration of the fixed point operator does not in general yield convergence, since it is a non-contractive mapping.[6] Instead, we have defined a procedure based on Newton's method for nonlinear systems of equations[7] which is depicted on figure 6. This necessitates the Jacobian matrix of the fixed point operator and is equivalent to iterating the following fixed point function:

$$\vec{\rho}_{out} = \vec{h}(\vec{\rho}_{in}) = \vec{\rho}_{in} + (\mathbf{J_g}(\vec{\rho}_{in}) - \mathbf{I})^{\dagger}(\vec{\rho}_{in} - \vec{\mathbf{g}}(\vec{\rho}_{in})) \quad (14)$$

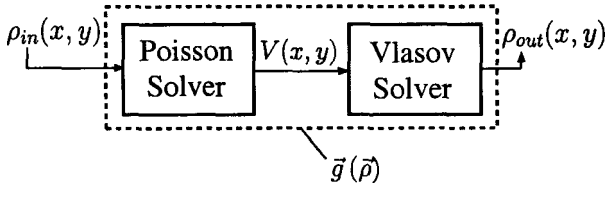

Fig. 5 Fixed Point Operator Comprised of Both the Poisson and Vlasov Solvers.

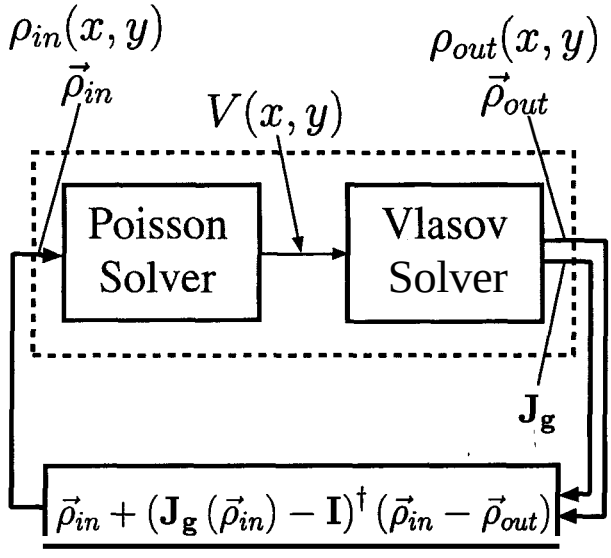

Fig. 6 Tikhonov-regularized Newton Iterative Poisson/Vlasov Procedure

where the symbol † represents a regularized inversion based on column normalization and Tikhonov regularization,[8] both of which are necessary to filter out the errors introduced by the Vlasov solver. These errors origniate from to the finite precision with which densities are computed, combined with the fact that like numbers are subtracted to obtain the net charge density in the pre-sheath where the ion and electron densities are very close to each other. $\mathbf{J_g}(\vec{\rho}_{in})$ is the Jacobian matrix of operator $\vec{\mathbf{g}}(\cdot)$ evaluated at $\vec{\rho}_{in}$. If there are N unknowns (N charge nodes), the Jacobian matrix is a $N \times N$ matrix and is defined by:

$$\mathbf{J}_{(i,j)} = \frac{\partial g_i}{\partial \rho_j}, \quad i = 1,\ldots,N, \quad j = 1,\ldots,N. \quad (15)$$

Solving equation (14) is equivalent to finding the fixed point of the linearized operator $\vec{\mathbf{g}}$ near an operating point $\vec{\rho}_{in}$. Successive linearizations leads to the solution of the nonlinear problem. Using finite differences to compute an approximation for **J**, would be prohibitively expensive computationally. Instead, direct computation of **J**, is performed. This involves combining the Jacobians of every sample of the velocity distribution function that was taken at that particular iteration, replicating all the operators that were applied to those sample results. To obtain the Jacobians of velocity distribution samples, the analytical Jacobians obtained at the outer boundary using equation (1) are propagated and transformed along each particle trajectory.

Software Implementation

The iterative resolution high-level algorithm and the Poisson solver, both fairly light computationally, were implemented in *Matlab*. The Vlasov solver, being much heavier computationally, was implemented in *Fortran* 90 using a parallel processing

At this location, the integral could be performed accurately over a disk of radius:

$$\Delta v = \sqrt{\frac{2eK_{max}}{m_{e,i}}} = \sqrt{\frac{2e\kappa T_{e,i}}{m_{e,i}}} \qquad (4)$$

centered around the center of the Maxwellian distribution, located at $v_x = v_d, v_y = 0$. This disk is located between **2** rings of velocity magnitudes $|v_{min}|$ and $|v_{max}|$ given by:

$$v_{min} = \max(0, v_d - \Delta v) \quad v_{max} = v_d + \Delta v \qquad (5)$$

which correspond to kinetic energy values (expressed in units of eV's) of $K_{min} = \frac{m_{e,i}v_{min}^2}{2e}$ and $K_{max} = \frac{m_{e,i}v_{max}^2}{2e}$. Since energy is conserved along particle trajectories, we can infer the following limits of integration along the kinetic energy axis at a location situated at a potential V (in volts):

$$K_{min} = \max\left(0, \frac{m_{e,i}v_{min}^2}{2e} - \frac{q_{e,i}}{e}V\right) \qquad (6)$$

$$K_{max} = \max\left(0, \frac{m_{e,i}v_{max}^2}{2e} - \frac{q_{e,i}}{e}V\right) \qquad (7)$$

which can be expressed in terms of velocity magnitudes:

$$v_{min} = \sqrt{\frac{2eK_{min}}{m_{e,i}}} \quad v_{max} = \sqrt{\frac{2eK_{max}}{m_{e,i}}} \qquad (8)$$

Figure **4** shows the corresponding velocity domains of integration. The ***2-D*** integration is performed in cylindrical coordinates, using **2** embedded 7-point adaptive Newton-Cotes quadrature rules (the integration routine "DQNC79" was used from the SLATEC Common Mathematical Library, distributed by Netlib at *www.netlib.org*). The dynamic integration routine is performed at all nodes on the charge density mesh.

The process described above constitutes the "Vlasov solver" which computes the charge density distribution from a known potential distribution. It accounts for the largest part of the computational complexity of the technique presented here.

Poisson solver

The Poisson solver computes a potential distribution from **a** given plasma charge density distribution, accounting for the surface charge on the tether surface **as** well **as** the induced surface charge on the outer boundary, which is simply modeled **as** a metallic wall.

Poisson's equation and the outer boundary condition:

$$\epsilon_0 \nabla^2 V(x,y) = \rho(x,y), \quad V|_{r=r_{bc}} = 0 \text{ Volts} \qquad (9)$$

can be solved for to obtain the first of two contributions to the complete potential distribution, generated

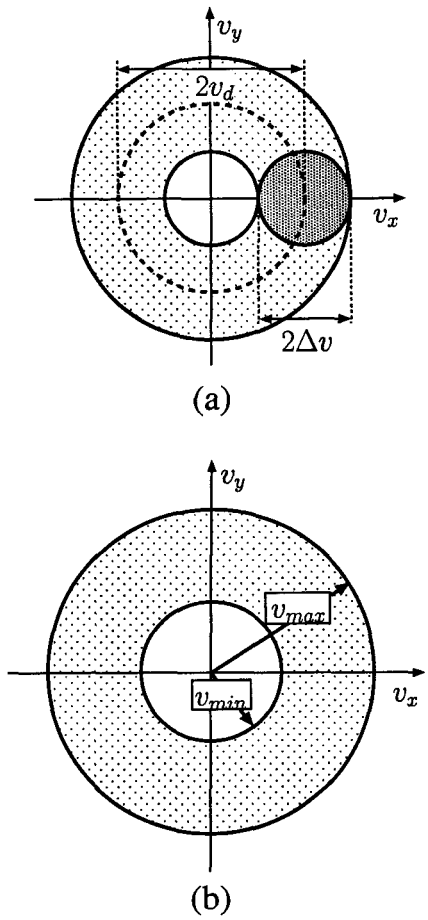

Fig. 4 (a) Domain of Integration of the Velocity Distribution Function at the Outer Boundary ($V = 0$). The shaded region corresponds to the bulk of the drifting Maxwellian population. (b) Domain of Integration of the Velocity Distribution Function at any Given Point in Space.

by the plasma charge distribution **as** well as the induced surface charges on the outer boundary shell:

$$V_{plasma}(r,\theta) = \frac{-1}{4\pi\epsilon_0}\int\int r'dr'd\theta'\rho(r',\theta') \times \left[\ln\left(\frac{r^2 + r'^2 - 2r'r\cos(\theta-\theta')}{r_{bc}^2 + r'^2 - 2r'r_{bc}\cos\theta'}\right) - \ln\left(\frac{r^2 + (r_{bc}^2/r')^2 - 2(r_{bc}^2/r')r\cos(\theta-\theta')}{r_{bc}^2 + (r_{bc}^2/r')^2 - 2(r_{bc}^3/r')\cos\theta'}\right)\right] \qquad (10)$$

where the first term in the bracketed expression represents the direct contribution from a ***2D*** element of charge. The second term represents the contribution from the corresponding induced surface charge on the outer shell and was obtained using to the Method of Images.[4] The location $(r = r_{bc}, \theta = 0)$ was used **as** the reference for potential.

A point-matching technique is then used in order to find the required surface charge distribution on the

well suited for a log(r)-based sampling scheme. In the flowing cases, the sheath structure is no longer circular. As the flow energy is increased, it departs from a circular symmetry to acquire an elongated shape. Therefore, in order to achieve a better consistency in our flowing cases, we should implement a sampling scheme that seeks to adapt itself to the shape of the sheath.

Present Status and Conclusions

A novel approach based on kinetic theory was presented for the 2-D modeling of the tether problem. One of the important difficulties in finding self-consistent solutions for such problems is finding an appropriate algorithm that will yield convergence in order to find the fixed point of the Vlasov-Poisson operator.' To address this issue, a new numerical algorithm for computing the Jacobian matrix of the Vlasov-Poisson operator was developed which allowed use of the Newton iterative method for non-linear systems.

The proposed algorithm was validated with the well-documented Langmuir cylindrical probe theory in the non-flowing Orbital Motion Limit regime. Flowing plasma test cases were also studied, and showed a trend for collection current below the OML regime, consistent with recent experimental results.[3] However, Poisson/Vlasov consistency showed to be increasingly difficult to achieve as the flow energy increased. This is likely to be due to the logarithmic radial spacing scheme based on circular symmetry for the charge and potential samples. Further developments of an adaptive meshing scheme should aleviate these issues. In addition, although our basic algorithm allows arbitrary tether cross-section geometries, it was only tested so far with circular cross-sections. Future tests will address non-circular cross-sections.

Acknowledgments

E.C. acknowledges the scholarship support of the Horace H. Rackham School of Graduate Studies at the University of Michigan, the Natural Sciences and Engineering Research Council of Canada and the Communications Research Centre(Canada).

References

[1]Laframboise, J., Theory of Sperical and Cylindrical *Langmuir* Probes *in* a *Collisionless, Maxwellian* Plasma at Rest, Ph.D. thesis, University of Toronto, 1966.

[2]Sanmartín, J. and Estes, R., "The Orbital-Motion-Limited Regime of Cylindrical Langmuir Probes," Physics of Plasmas, Vol. 6, No. 1, 1999, pp. 395-405.

[3]Gilchrist, B. E., Bilkn, S. G., Choinière, E., Gallimore, A. D., and Smith, T. B., "Analysis of Chamber Simulations of Long Collecting Probes in High-speed, Dense Plasmas," IEEE *Transactions* on Plasma Science, 2002, paper accepted for publication in May 2002.

[4]Cheng, D. K., Field and wave electromagnetics, Addison-Wesley Pub. Co., 1989.

[5]Stutzman, W. L. and Thiele, G. A., Antennna Theory and Design, John Wiley & Sons, 1981.

[6]Sikorski, K. A., Optimal *Solution* of Nonlinear Equations, Oxford University Press, 2001.

[7]Burden, R. L., Numerical Analysis, PWS-KENT Publishing Company, 4th ed., 1989.

[8]Hansen, C., Regularization Tools - A Matlab Package for Analysis and Solution of Discrete Ill-Posed Problems, University of Denmark, 2001.

'Brace, L. H.,"Langmuir Probe Measurements in the Ionosphere," Measurement Techniques in Space Plasmas: Particles, 1998, pp. 23-34, Geophysical Monograph.

scheme based on the *Parallel Virtual Machine* library (www.epm.ornl.gov/pvm/pvm_home.html). A pool of about 100 Sun Sparc Ultra-5 and Ultra-10 workstation nodes are used concurrently to form the Vlasov solver. This allows iteration times anywhere from 25 seconds to 5 minutes (per iteration), with most problems requiring from **30** to 100 iterations for adequate convergence.

Simulation Results & Validation

Non-flowing plasma - Langmuir Probe sweep

In order to gain confidence in this modeling tool, some validation runs were performed with simple cases that can be checked against known theories. Figure 7 presents the results obtained for the I-V curve of a Langmuir cylindrical probe of radius $r_0 = 0.14$ mm in a Xenon plasma ($m_i = 2.18 \times 10^{-25}$ kg) with a density $n_0 = 1.42 \times 10^{16}$ m^{-3} and a temperature of $T_e = T_i = 1.07$ eV. The I-V curve has been split in two separate parts to emphasize the small variation in the ion saturation region.

In both the ion and electron saturation regions, our results are in good agreement with the Orbit Motion Limit theory, which is valid in the present case for sufficiently large voltages due to the fact that the probe radius is fairly small in terms of the Debye length ($\lambda_d = 0.062$ mm). The OML expression used for comparison is:[2]

$$I_{oml} = 2r_0 e n_0 \sqrt{\frac{2eT_e}{m_{e,i}}} \sqrt{1 + \frac{|V|}{T_e}} \qquad (16)$$

where m_e and m_i were used, respectively, in the electron and ion saturation regions.

The behavior of the response in the electron retardation region (near V = 0 Volts) is also in excellent agreement with Langmuir cylindrical probe theory, as can be seen on figure 7. The expression used for comparison here is:[9]

$$I_e = 2\pi n_0 r_0 e \sqrt{\frac{eT_e}{2\pi m_e}} \exp \frac{V}{T_e} \qquad (17)$$

This initial validation of the proposed algorithm confirms that the important physical mechanisms involved are being accurately represented in the model.

Flowing plasma results

Here we consider results for a simulated probe of radius $r_0 = 0.14$ mm biased at 20 volts in a flowing Xenon plasma with a background number density of $n_0 = 3.56 \times 10^{15}$ m^{-3}. Figures 8 through 11 present, in graphical form, the results that were obtained for ion flow energies of 0 eV (non-flowing case), 1 eV, 2 eV and **4** eV. On these figures, the action of the Poisson solver is shown by the "Net charge ρ_{in}" to "Potential" transformation. The "Potential" to "Ion density" and

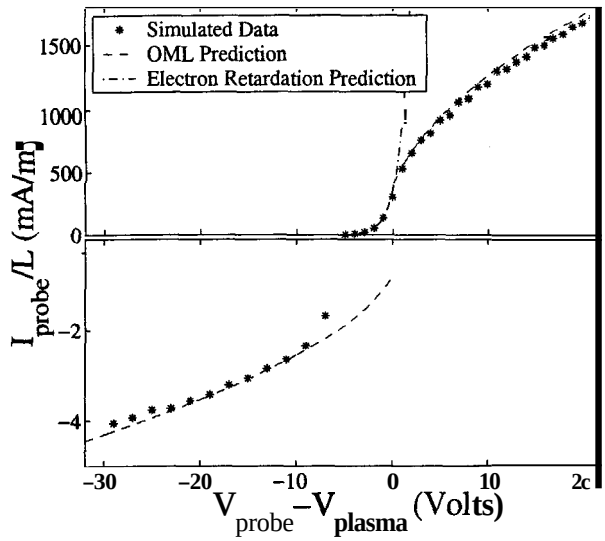

Fig. 7 I-V Characteristic Curve of a Langmuir Probe. Note that the ion and electron saturation regions are displayed on two separate linear scales, since the variations in the ion saturation regions are very small.

"Electron density" transformation constitutes the application of the Vlasov solver. The "Net charge ρ_{out}" graph is simply obtained by combining the ion and electron density distributions. The consistency of the results is assessed by comparing the input and output charge density distributions (ρ_{in} and ρ_{out}) that were, respectively, fed in and produced by the Poisson-Vlasov fixed point operator discussed earlier. Values for the relative error between the input and output charge density distributions ($||\rho_{out} - \rho_{in}||/||\rho_{in}||$) are also shown on the figures.

As in the previous section, it can be seen on figure 8 that the amount of current collected in the non-flowing case **(0.431 A)** agrees very well with the OML prediction **(0.433 A),** as expected. The currents obtained for more energetic ion flows are lower than the OML prediction however. This is consistent with recent **ex**perimental measurements performed on probes in a flowing plasma.' Finally, for the flowing cases, the ion and electron number density distributions clearly show a depression in the wake region, **as** is expected, while maintaining quasi-neutrality in the presheath region, part of which was included in the computational domain. This provides further qualitative confirmation of the validity of our results.

As the flow energy is increased, the rise in the relative error $||\rho_{out} - \rho_{in}||/||\rho_{in}||$ shows that it is more and more difficult to obtain a consistent solution to the Poisson/Vlasov equations. The current status of our research indicate that this is probably a consequence of forcing the charge and potential samples to be spaced in a logarithmic fashion along **r.** The non-flowing case accomodates itself easily of this constraint, because the sheath structure is circular in this case and is therefore

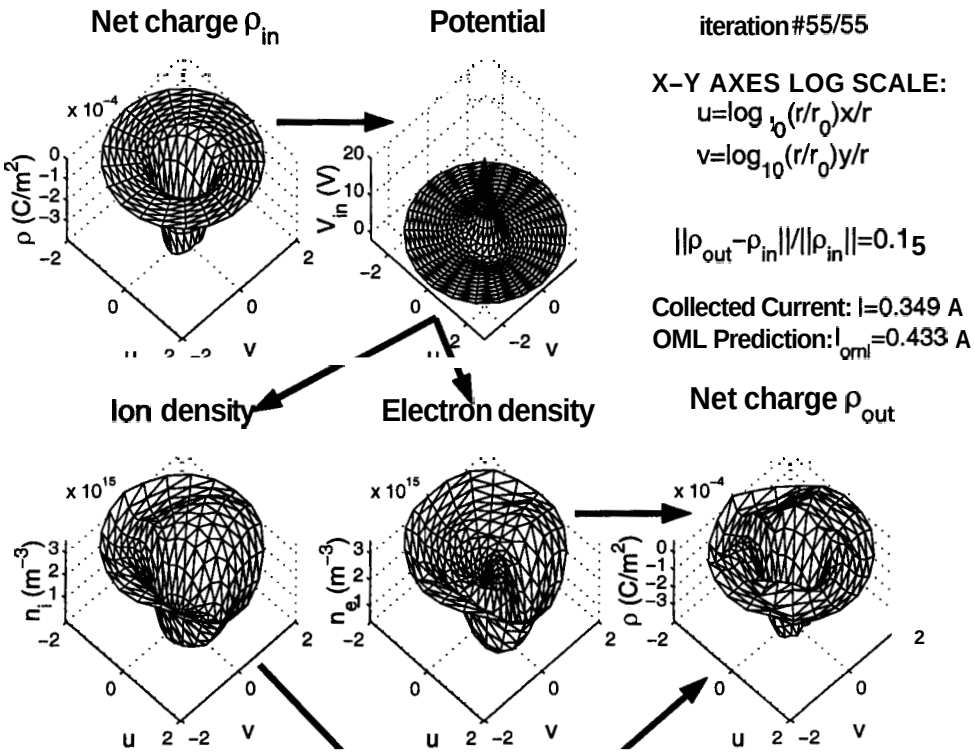

Fig. 10 Results for a probe of radius $r_0 = 0.14$ mm biased at 20 volts in a Xenon plasma with a background number density $n_0 = 3.56 \times 10^{15}\ m^{-3}$ and an ion flow energy of 2 eV.

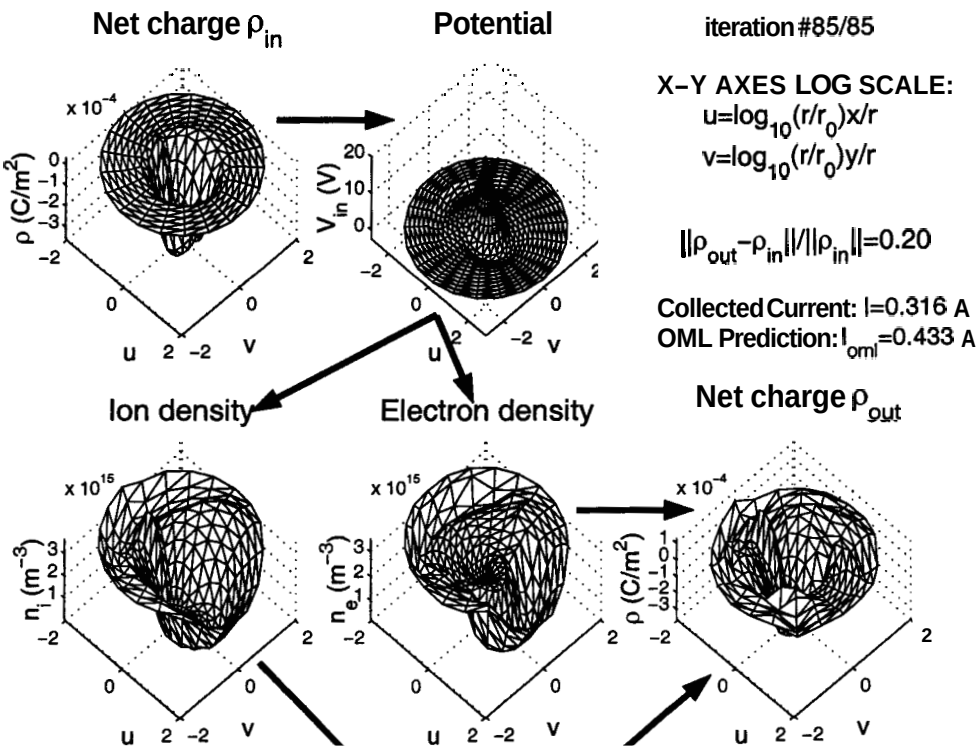

Fig. 11 Results for a probe of radius $r_0 = 0.14$ mm biased at 20 volts in a Xenon plasma with a background number density $n_0 = 3.56 \times 10^{15}\ m^{-3}$ and an ion flow energy of 4 eV.

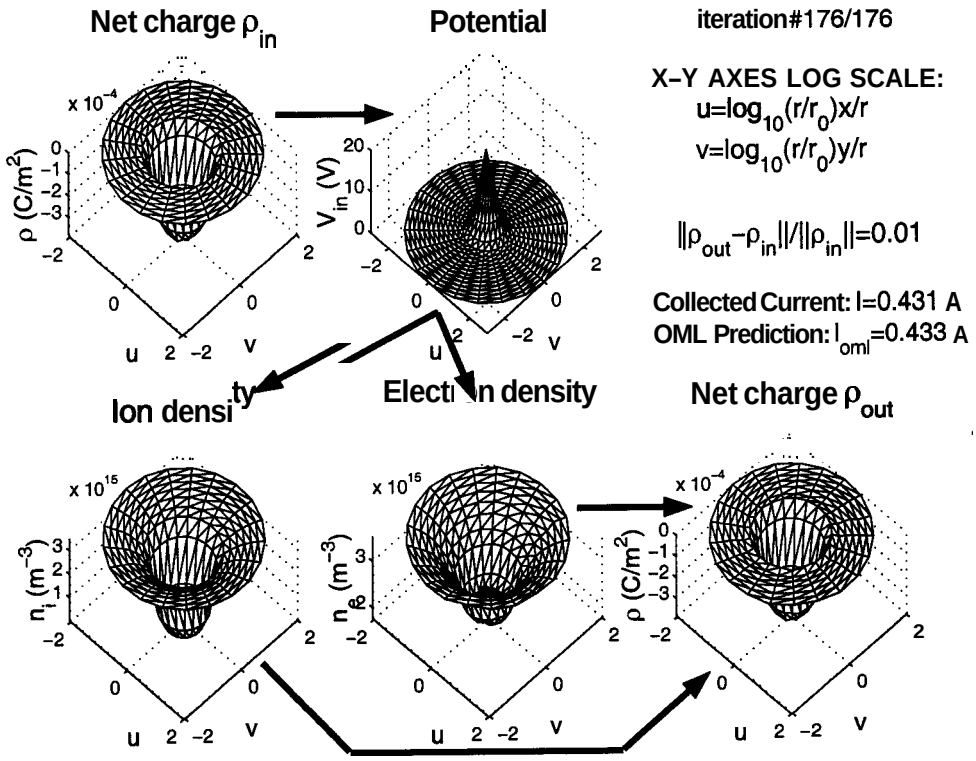

Fig. 8 Results for a probe of radius $r_0 = 0.14$ mm biased at 20 volts in a non-flowing Xenon plasma with a background number density $n_0 = 3.56 \times 10^{15}\ m^{-3}$

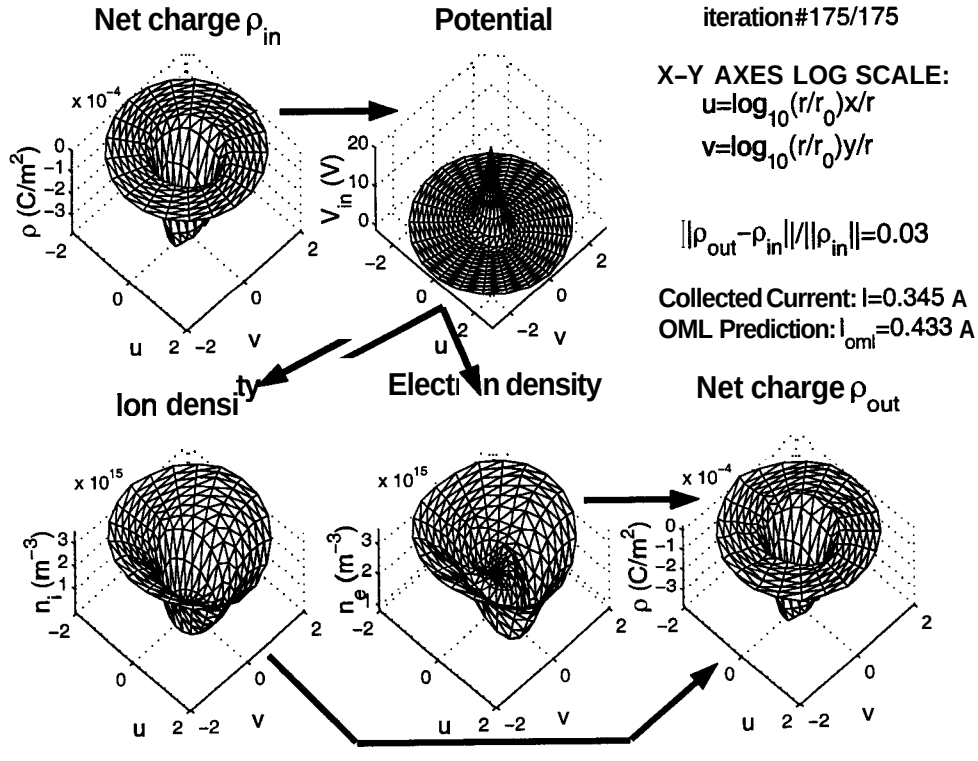

Fig. 9 Results for a probe of radius $r_0 = 0.14$ mm biased at 20 volts in a Xenon plasma with a background number density $n_0 = 3.56 \times 10^{15}\ m^{-3}$ and an ion flow energy of 1 eV.